Published in Journal of Inorganic Biochemistry 100, issue 3, 316-330, 2006
which should be used for any reference to this work

Structures, spectra, and DNA-binding properties of mixed ligand copper(II) complexes of iminodiacetic acid: The novel role of diimine co-ligands on DNA conformation and hydrolytic and oxidative double strand DNA cleavage

Balaraman Selvakumar [a], Venugopal Rajendiran [a], Palanisamy Uma Maheswari [a], Helen Stoeckli-Evans [b], Mallayan Palaniandavar [a,*]

[a] *School of Chemistry, Bharathidasan University, Tiruchirappalli 620 024, Tamilnadu, India*
[b] *Institut de Chimie, Universté de Neuchâtel, Avenue de Bellevaux 51, C.P.2, CH-2007 Neuchâtel, Switzerland*

Abstract

The coordination geometry around copper(II) in [Cu(imda)(phen)(H_2O)] (**1**) (H_2imda = iminodiacetic acid, phen = 1,10-phenanthroline) is described as distorted octahedral while those in [Cu(imda)(5,6-dmp)] (**2**) (5,6-dmp = 5,6-dimethyl-1,10-phenanthroline) and [Cu(imda)(dpq)] (**3**) (dpq = dipyrido-[3,2-*d*:2′,3′-*f*]-quinoxaline) as trigonal bipyramidal distorted square-based pyramidal with the imda anion facially coordinated to copper(II). Absorption spectral (K_b: **1**, $0.60 \pm 0.04 \times 10^3$; **2**, $3.9 \pm 0.3 \times 10^3$; **3**, $1.7 \pm 0.5 \times 10^4$ M^{-1}) and thermal denaturation studies (ΔT_m: **1**, 5.70 ± 0.05; **2**, 5.5 ± 10; **3**, 10.6 ± 10 °C) and viscosity measurements indicate that **3** interacts with calf thymus DNA more strongly than **1** and **2**. The relative viscosities of DNA bound to **1** and **3** increase while that of DNA bound to **2** decreases indicating formation of kinks or bends and/or conversion of B to A conformation as revealed by the decrease in intensity of the helicity band in the circular dichroism spectrum of DNA. While **1** and **3** are bound to DNA through partial intercalation, respectively, of phen ring and the extended planar ring of dpq with DNA base stack, the complex **2** is involved in groove binding. All the complexes show cleavage of pBR322 supercoiled DNA in the presence of ascorbic acid with the cleavage efficiency varying in the order **3** > **1** > **2**. The highest oxidative DNA cleavage of dpq complex is ascribed to its highest Cu(II)/Cu(I) redox potential. Oxidative cleavage studies using distamycin reveal minor groove binding for the dpq complex but a major groove binding for the phen and 5,6-dmp complexes. Also, all the complexes show hydrolytic DNA cleavage activity in the absence of light or a reducing agent with cleavage efficiency varying in the order **1** > **3** > **2**.

Keywords: Cu(II) complexes; Iminodiacetic acid; Diimines; Circular dichroism; Electrochemistry; Oxidative and hydrolytic DNA cleavage

1. Introduction

A precise understanding of the DNA-binding properties of metal complexes are driven by numerous motivations, which include therapeutic approaches, study of nucleic acid conformations and new tools for nanotechnology [1–4]. The characterization of DNA recognition by small redox- or photoactive transition metal complexes has been substantially aided by studying the DNA cleavage activity [5–8]. Double-strand breaks in duplex DNA are thought to be more significant sources of cell lethality than are single strand breaks, as they appear to be less readily repaired by DNA repair mechanisms [9–11]. A number of copper(II) complexes have been used as candidates for mediation of strand scission of duplex DNA [12,13] and as probes of DNA structure

* Corresponding author.
E-mail address: palani51@sify.com (M. Palaniandavar).

in solution [14–17]. Sigman and co-worker have shown that copper complexes of 1,10-phenanthroline (phen) act as effective chemical nuclease with a high preference for double-stranded DNA in the presence of molecular oxygen and a reducing agent [18]. A number of metal complexes have been shown to hydrolyze phosphate ester [19] as well as RNA with varying efficiencies [20]; however, they are unable to hydrolyze the phosphate diester backbone of DNA. Burstyn and co-worker reported that copper(II)–macrocyclic triamine complexes promote the hydrolytic cleavage of plasmid DNA [21]. In recent years, there has been substantial interest in the design and study of Lewis acidic, potential redox and spectroscopically active Cu(II/I) complexes of synthetic and naturally occurring ligands as nuclease mimics [22–25] and in fact, a few copper(II) complexes have been shown to be capable of mediating non-random double-strand cleavage of plasmid DNA.

The present work stems from our continuous interest in defining and evaluating the key DNA-binding interactions of copper(II) complexes of diimine ligands [26–29] and also from our current efforts to explore the relationship between structure and nuclease activity of copper(II) complexes [30,31]. In this report, we explore the DNA-binding properties of a series of copper(II) complexes of the type [Cu(imda)(diimine)], where H_2imda = iminodiacetic acid and diimine = 1,10-phenanthroline (phen), 5,6-dimethyl-1,10-phenanthroline (5,6-dmp) and dipyrido-[3,2-*d*:2′,3′-*f*]-quinoxaline (dpq). The rationale behind the design of the complexes is that the carboxylate groups of H_2imda can interact with sugar hydroxyl groups of DNA and supply the recognition elements like amine and carboxylate groups of amino acids and protein moieties thus leading to the selective control of the metal chelate-nucleobase recognition process. In fact, a variety of mixed ligand copper(II) complexes having imda anion and its derivatives serve as bioinorganic model compounds to illustrate conformational changes at the protein conformation for metal–protein centers in the absence or presence of appropriate substrates [32]. Also, the incorporation of methyl groups on the 5,6 positions of the phen ring would provide a hydrophobic recognition element [33]. We propose to assess the effect of varying the ring size and hydrophobicity of diimine co-ligands on the DNA-binding structure and hydrolytic cleavage activity of the complexes using a variety of approaches and also their ability to effect DNA cleavage has been probed. The X-ray crystal structures of all the present complexes have been successfully determined to aid in understanding the DNA-binding characteristics and hence the chemical principles underlying site-specific DNA recognition in biological systems. It is remarkable that the present complexes are efficient in bringing about the oxidative as well as the rare hydrolytic cleavage of DNA and that the dpq complex alone has the potential to cleave DNA double strand.

2. Experimental section

2.1. Materials

Copper acetate monohydrate (Sisco-Chem), 1,10-phenanthroline (Merck), iminodiacetic acid, 5,6-dimethyl-1,10-phenanthroline (Aldrich), calf-thymus (CT) DNA (Sigma), pBR322 supercoiled plasmid DNA, agarose (Genei). The ligand dipyrido-[3,2-*d*:2′,3′-*f*]-quinoxaline was synthesized by Hambly et al. [34]. Ultrapure Milli Q water (18.3 μΩ) was used for all experiments. The commercial solvents were distilled and then used for preparation of complexes.

2.2. Synthesis of complexes

2.2.1. Synthesis of [Cu(imda)(phen)(H_2O)] (**1**)

This complex was synthesized by adding to a methanol:water (4:1) solution of 1,10-phenanthroline (0.198 g, 1 mmol) and iminodiacetic acid (0.133 g, 1 mmol) which was deprotonated by NaOH (1 mmol equivalent), to a solution of copper(II) acetate (0.199 g, 1 mmol) in aqueous methanol solution and then stirred at 40 °C for 1 h. The resulting solution was filtered and kept aside for crystallization by slow evaporation at room temperature. The blue hexagonal crystals suitable for X-ray diffraction were collected by suction filtration. Anal. Calcd. for [Cu(phen)(imda)(H_2O)]: C, 48.92; H, 3.85; N, 10.70. Found: C, 48.72; H, 3.80; N, 10.59%.

2.2.2. Synthesis of [Cu(imda)(5,6-dmp)] (**2**)

This complex was prepared by employing the procedure for **1** and using 5,6-dimethyl-1,10-phenanthroline instead of 1,10-phenanthroline. The blue colored crystals suitable for X-ray diffraction were obtained on slow evaporation of a concentrated solution of the complex. Anal. Calcd. for [Cu(5,6-dmp)(imda)]: C, 53.66; H, 4.25; N, 10.43. Found: C, 53.80; H, 4.10; N, 10.13%.

2.2.3. Synthesis of [Cu(imda)(dpq)] (**3**)

This complex was isolated employing the procedure adopted for obtaining **1** and using dipyrido-[3,2-*d*:2′,3′-*f*]-quinoxaline instead of 1,10-phenanthroline. The blue colored needle shaped crystals suitable for X-ray diffraction were obtained on slow evaporation of a concentrated solution of the complex. Anal. Calcd. for [Cu(dpq)(imda)]: C, 50.65; H, 3.07; N, 16.41. Found: C, 50.53; H, 2.95; N, 16.47%.

2.3. Methods and instrumentation

Disodium salt of calf-thymus (CT) DNA was stored at 4 °C. Solutions of DNA in the buffer 50 mM NaCl/5 mM Tris–HCl (pH 7.1) in water gave the ratio of UV absorbance at 260 and 280 nm, A_{260}/A_{280}, of 1.9 [35] indicating that the DNA was sufficiently free of protein. Concentrated stock solutions of DNA (13.5 mM) were prepared in buffer

and sonicated for 25 cycles, where each cycle consisted of 30 s with 1 min intervals. The concentration of DNA measured by using its extinction coefficient at 260 nm ($6600\ cm^{-1}$) after 1:100 dilutions. Stock solutions were stored 4 °C and used no more than 4 days. Supercoiled plasmid pUC19 DNA was stored at −20 °C.

Concentrated stock solutions of metal complexes were prepared by dissolving in methanol:water (4:1) of metal complexes and diluted suitably with corresponding buffer to required concentrations for all the experiments. For absorption, emission, circular dichroic spectral experiments the DNA solutions were pretreated with the solutions of metal complexes to ensure no change in the concentration of the metal complexes. The absorption spectra were recorded on a Varian Cary 300 Bio UV–Vis spectrophotometer using cuvettes of 1 cm path length.

Infra-red spectra of the complexes were recorded as KBr pellets on Perkin–Elmer FT-IR spectrometer. Electron paramagnetic resonance (EPR) spectra of the mixed ligand complexes were obtained on a Varian E 112 EPR spectrometer. The spectra were recorded for the solutions of the compound in double-distilled methanol at room temperature (RT) as well as at liquid nitrogen temperature (LNT). DPPH was used as the field marker. Cyclic voltammetry (CV) and differential pulse voltammetry (DPV) were performed using a three-electrode cell configuration. A platinum sphere, a platinum plate and $Ag(s)/AgNO_3$ were used as working, auxiliary and reference electrodes, respectively. The supporting electrolyte used was NBu_4ClO_4. Platinum sphere electrode was sonicated for two minutes in dilute nitric acid, dilute hydrazine hydrate and then in double-distilled water to remove the impurities. The temperature of the electrochemical cell was maintained at 25 ± 0.2 °C by a cryocirculator (HAAKE D8 G). The solutions were deoxygenated by bubbling research grade nitrogen and an atmosphere of nitrogen was maintained over the solution during measurements. The $E_{1/2}$ values were observed under identical conditions for various scan rates. The instruments utilized included an EG&G PAR 273 Potentiostat/Galvanostat and an IBM PS2 computer along with EG&G M270 software to carry out the experiments and to acquire the data.

Absorption spectral titration experiments were performed in Varian Cary 300 Bio UV–Vis spectrophotometer. Maintaining a constant concentration of the complex while varying the nucleic acid concentration. This was achieved by dissolving an appropriate amount of the metal complex and DNA stock solutions while maintaining the total volume constant (1 ml). This result in a series of solutions with varying concentrations of DNA but with a constant concentration of the complex. The absorbance (A) of the most red-shifted band of each investigated complex was recorded after successive additions of CT DNA.

Emission intensity measurements were carried out using Jasco F 6500 spectrofluorometer. The tris buffer was used as a blank is make preliminary adjustments. The excitation wavelength was fixed and the emission range was adjusted before measurements. DNA was pretreated with ethidium bromide in the ratio [NP/EthBr] = 1 for 30 min at 27 °C. The metal complexes were then added to this mixture and their effect on the emission intensity was measured.

For viscosity measurements a Schott Gerate AVS 310 automated viscometer was thermostated at 25 °C in a constant temperature bath. The concentration of DNA was 500 μM in NP and the flow times were noted from the digital timer attached with the viscometer ($1/R = [Cu]/[DNA] = 0.5$). Thermal denaturation studies were performed by Varian Cary UV–Vis spectrophotometer. DNA melting experiments were carried out by monitoring the absorption (260 nm) of CT DNA (160 μM) at various temperatures, in both the absence and presence of (16 μM) each investigated complex. The melting temperature (T_m) and the curve width σ_T (= temperature range between which 10% to 90% of the absorption increase occurred) were calculated.

Circular dichroic spectra of DNA were obtained by using JASCO J-716 spectropolarimeter equipped with a peltier temperature control device. All experiments were done using a quartz cell of 1 or 0.2 cm path length. Each CD spectrum was collected after averaging over at least 4 accumulations using a scan speed of 100 nm min^{-1} and a 1 s response time. Machine plus cuvette baselines were subtracted and the resultant spectrum zeroed 50 nm outside the absorption bands.

The hydrolytic cleavage experiments were performed using SC pBR322 DNA in 10 mM HEPES, pH 8.1. The reactions were performed incubating DNA (12 μM base pairs) at 37 °C in the presence/absence of metal complexes (0.5 mM) for the indicated time. For anaerobic experiments, deoxygenated water and anaerobic stock solutions were prepared. In order to examine if hydroxyl radicals were present, hydroxyl radical scavengers such as DMSO (0.8 mM) were introduced. The oxidative cleavage experiments were performed using supercoiled pBR322 plasmid DNA (Form I, 2 μl, 10 μM) in Tris–HCl buffer (50 mM) with 50 mM NaCl (pH 7.1) was treated with the metal complex (30 μM) and ascorbic acid (10 μM) followed by dilution with the Tris–HCl buffer to a total volume of 20 μl. The samples were incubated for 0.5 h at 37 °C. A loading buffer containing 25% bromophenol blue, 0.25% xylene cyanol, 30% glycerol (3 μl) was added and electrophoresis performed at 40 V for 3 h in Tris–Acetate–EDTA (TAE) buffer using 1% agarose gel containing 1.0 μg/ml ethidium bromide. The cleavage of DNA was monitored using agarose gel electrophoresis. The gel was visualized by photographing the fluorescence of intercalated ethidium bromide under a UV illuminator. The cleavage efficiency was measured by determining the ability of the complex to convert the supercoiled DNA (SC) to nicked circular form (NC) and linear form. After electrophoresis the proportion of DNA in each fraction was estimated quantitatively from the intensities of the bands using UVP Bioimaging – GDS-8000 Gel Documentation System using the Labwork software. The fraction of the original

Table 1
Crystal data and structure refinement details for **1**, **2** and **3**

	1	**2**	**3**
Empirical formula	$C_{16}H_{18}CuN_3O_{6.5}$	$CuC_{18}H_{17}N_3O_4 \cdot 5.5H_2O$	$CuC_{18}H_{16}N_5O_{6.5}Cu$ $C_{18}H_{16}N_5O_4 \cdot 2.5(H_2O)$
Formula weight	419.87	501.97	469.9
Crystal system	Triclinic	Triclinic	Triclinic
Space group	$P\bar{1}$	$P3_1$	$P\bar{1}$
a (Å)	6.7653(5)	13.2103(5)	7.9465(7)
b (Å)	10.6008(7)	13.2103(5)	15.3837(15)
c (Å)	11.4385(9)	21.5182(10)	16.5664(15)
α (°)	95.736(6)	90	69.28(7)
β (°)	91.646(6)	90	79.52(7)
γ (°)	92.528(6)	120	78.755(7)
V (Å^3)	814.99(10)	3252.1(2)	1843.7(3)
Z	2	6	4
Mo Kα, λ (Å)	0.71073	0.71073	0.71073
D_{calc} (g cm^{-3})	1.711	1.538	1.693
Goodness-of-fit on F^2	1.064	0.953	0.926
No. of reflections *Measured*	1564	12807	7919
R^a	0.0227	0.0418	0.0359
R^b	0.0590	0.055	0.0593

[a] $R = \sum||F_o| - |F_c||/\sum|F_o|$.
[b] $R = \{\sum w[(F_o^2 - F_c^2)^2/\sum w[(F_o^2)^2]\}^{1/2}$.

supercoiled DNA converted to the nicked and linear form at the end of the reaction was calculated after correcting for the low level of NC present in the original sample and the low affinity of ethidium bromide binding to SC compared to nicked and linear forms of DNA [36]. Inhibition reactions were carried out by prior incubation of the SC pBR322 DNA (10 μM) with ethanol (1 M), sodium azide (100 mM), superoxide dismutase (10 U) and distamycin (100 μM).

2.4. Crystallographic data collection and structure analysis

Experimental details of the X-ray analysis are provided in Table 1. Suitable crystals were obtained and intensity data were collected at 153 K on a Stoe Image Plate Diffraction System using Mo Kα graphite monochromated radiation. The structure was solved by X-ray crystallography-Direct method using the programme SHELXS-97. The refinement and all further calculations were carried out using SHELXS-97.

3. Results and discussion

3.1. Structures and spectral and redox properties of the complexes

The mixed ligand copper(II) complexes of iminodiacetic acid (H_2imda) as the primary ligand and the diimines 1,10-phenanthroline (phen), 5,6-dimethyl-1,10-phenanthroline (5,6-dmp) and dipyridoquinoxaline (dpq) as the co-ligands have been synthesized in aqueous methanol solution using hydrated copper(II) acetate. All the complexes conform to the general formula [Cu(imda)(diimine)$(H_2O)_n$], where $n = 0$ (**2**,**3**), 1 (**1**), determined on the basis of elemental analysis and confirmed by the X-ray crystal structures. The infrared spectrum of H_2imda shows a medium intensity band in the range 3096–3036 cm^{-1}, which is assigned to ν(OH) of carboxylic acid group. On complex formation with copper(II) this band disappears indicating deprotonation of the acid followed by its co-ordination through carboxylate oxygen atoms. This is further supported by the shifts [37] in ν_{as}(COO) (1700 cm^{-1}) and ν_s(COO) (1400 cm^{-1}) bands of H_2imda, respectively, to 1638–1625 and 1407–1385 cm^{-1} in the complexes. Further, the difference between these two bands $\Delta\nu$ [ν_{as}(COO) − ν_s(COO)] of 238–247 cm^{-1} is typical of unidentate mode of coordination of carboxylate to copper(II) in all the complexes, which is confirmed by the X-ray crystal structures of the complexes. A strong band around 3440 cm^{-1} observed for **1** is assignable to ν(OH) of coordinated water.

3.1.1. Description of the crystal structures

*3.1.1.1. [Cu(imda)(phen)(H$_2$O)] (**1**).* An ORTEP representation of the structure of **1** including atom numbering scheme is shown in Fig. 1 and the selected bond lengths and bond angles are listed in Table 2. The asymmetric unit cell of the complex consists of two crystallographically independent complex molecules. The Cu(II) is located at

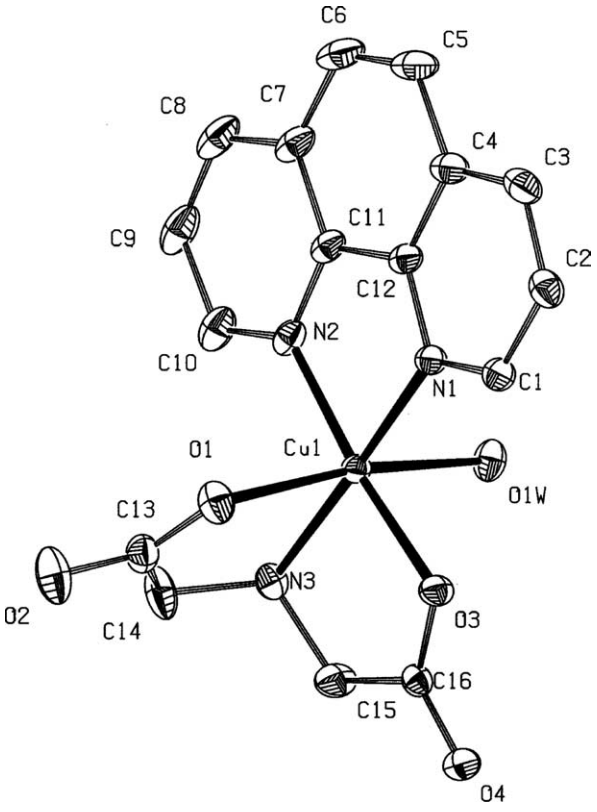

Fig. 1. ORTEP drawing of [Cu(imda)(phen)(H$_2$O)] (**1**) showing the atom numbering scheme and the thermal motion ellipsoids (50% probability level) for the non-hydrogen atoms. Hydrogen atoms are omitted for clarity.

Table 2
Selected interatomic distances (Å) and angles (°) for complexes **1**–**3**

Complex	Bond lengths		Bond angles	
1	Cu(1)–O(3)	1.9733(9)	O(3)–Cu(1)–N(1)	94.63(4)
	Cu(1)–N(1)	2.0110(10)	O(3)–Cu(1)–N(2)	173.91(4)
	Cu(1)–N(2)	2.0372(11)	N(1)–Cu(1)–N(2)	82.11(4)
	Cu(1)–N(3)	2.0458(10)	O(3)–Cu(1)–N(3)	85.49(4)
	Cu(1)–O(1)	2.3132(10)	N(1)–Cu(1)–N(3)	175.44(4)
	Cu(1)–O(1W)	2.3746(10)	N(2)–Cu(1)–N(3)	98.17(4)
			O(3)–Cu(1)–O(1)	90.18(4)
			N(1)–Cu(1)–O(1)	96.99(4)
			N(2)–Cu(1)–O(1)	95.31(4)
			N(3)–Cu(1)–O(1)	78.45(4)
			O(3)–Cu(1)–O(1W)	87.20(4)
			N(1)–Cu(1)–O(1W)	92.59(4)
			N(2)–Cu(1)–O(1W)	7.81(4)
			N(3)–Cu(1)–O(1W)	91.97(4)
			O(1)–Cu(1)–O(1W)	170.25(4)
2	Cu(1)–O(1)	1.931(3)	O(1)–Cu(1)–N(1)	91.48(14)
	Cu(1)–N(1)	1.998(4)	O(1)–Cu(1)–N(2)	166.00(16)
	Cu(1)–N(2)	2.045(4)	N(1)–Cu(1)–N(2)	81.90(14)
	Cu(1)–N(3)	2.045(4)	O(1)–Cu(1)–N(3)	85.69(14)
	Cu(1)–O(3)	2.254(4)	N(1)–Cu(1)–N(3)	177.12(16)
			N(2)–Cu(1)–N(3)	100.97(15)
	Cu(2)–O(21)	1.933(3)	O(1)–Cu(1)–O(3)	93.24(14)
	Cu(2)– N(21)	1.990(4)	N(1)–Cu(1)–O(3)	101.64(15)
	Cu(2)–N(22)	2.024(4)	N(2)–Cu(1)–O(3)	100.15(14)
	Cu(2)–N(23)	2.033(4)	N(3)–Cu(1)–O(3)	78.04(15)
	Cu(2)–O(23)	2.222(4)		
3	Cu(1)···O(4a)	2.889(2)	O(3)–Cu(1)–N(3)	91.23(8)
	Cu(1)–O(3)	1.9346(17)	O(3)–Cu(1)–N(2)	163.11(9)
	Cu(1)–N(3)	1.997(2)	N(3)–Cu(1)–N(2)	82.19(8)
	Cu(1)–N(2)	2.022(2)	O(3)–Cu(1)–N(1)	85.57(8)
	Cu(1)–N(1)	2.026(2)	N(3)–Cu(1)–N(1)	176.75(8)
	Cu(1)–O(1)	2.238(2)	N(2)–Cu(1)–N(1)	101.05(8)
			O(3)–Cu(1)–O(1)	93.50(8)
	Cu(2)–O(7)	1.9299(18)	(3)–Cu(1)–O(1)	98.48(8)
	Cu(2)–N(8)	2.003(2)	(2)–Cu(1)–O(1)	102.82(8)
	Cu(2)–N(7)	2.031(2)	(1)–Cu(1)–O(1)	81.16(8)
	Cu(2)–N(6)	2.040(2)		
	Cu(2)–O(5)	2.140(2)		

the center of a distorted octahedral coordination environment, which consists of secondary amine nitrogen (N3) and two oxygen atoms (O1, O3) from the *cis*-facially coordinated imda anion and two nitrogen atoms (N1, N2) from phen. The nitrogen atoms N1, N2 and N3 and the oxygen atom O1 occupy the corners of the square plane of the coordination octahedron and the oxygen atoms O1W and O1 occupy the axial positions at distances longer than the equatorial one (O3), which is a consequence of Jahn–Teller effect (two electrons in d_{z^2} orbital). Further, the axial Cu–O1 bond (2.313 Å) is shorter than the axial Cu–O1W bond (2.375 Å), as O1 atom is a part of the chelated imda anion. The Cu–N_{amine} bond [Cu–N3, 2.046 Å] is longer than the Cu–N_{phen} bonds [Cu–N1, 2.011, Cu–N2, 2.037 Å], which is expected of the sp^3 and sp^2 hybridizations of the amine and imine nitrogen atoms. The Cu–$N1_{phen}$ bond is shorter than the Cu–$N2_{phen}$ bond, as it is *trans* to the longer Cu–N3 bond (2.046 Å). The bond angles O1–Cu–O1W (170.2°), N1–Cu–N3 (175.4°) and O3–Cu–N2 (170.3°) show marked deviation from the ideal angle of 180° indicating that the coordination geometry is distorted octahedral.

*3.1.1.2. [Cu(imda)(5,6-dmp)] (**2**).* The ORTEP representation of the structure of **2**, including atom numbering scheme, is shown in Fig. 2 and the selected bond lengths and bond angles are listed in Table 2. The asymmetric unit cell of **2** consists of two crystallographically independent molecules of the complex. The copper atom in each molecule is coordinated by two carboxylate oxygen (O1, O3) and the tertiary amine nitrogen (N3) atoms of the *cis*-facially coordinated imda anion and two 5,6-dmp nitrogen atoms (N1, N2). The value of the structural index [38] τ of 0.19 [$\tau = (\beta - \alpha)/60$, where α = N1–Cu1–N3 = 177.1° and β = O1–Cu1–O3 = 166.0°; for perfect square pyramidal and trigonal bipyramidal geometries the τ values are zero and unity, respectively] reveals that the coordination geometry around copper(II) is best described as trigonal bipyramidal distorted square-based pyramidal (TBDSBP) [39–41] with the corners of the CuN_3O square plane being occupied by N1, N2 and N3 nitrogen and O1 oxygen atoms. The apical position is occupied by O3 oxygen atom at a distance of 2.254 Å, longer than the equatorial O1 atom (Cu–O1, 1.931 Å) as a consequence of the presence of two electrons in d_{z^2} orbital. The Cu–N_{amine} bond (Cu–N3, 2.045 Å) is longer than the *trans* Cu–N_{phen} bond [Cu–N1, 1.998 Å] formed by phen, which is expected of sp^3 and sp^2 hybridizations, respectively, of amine and imine nitrogen atoms. Interestingly, the Cu–$N1_{phen}$ bond (1.998 Å) is shorter than

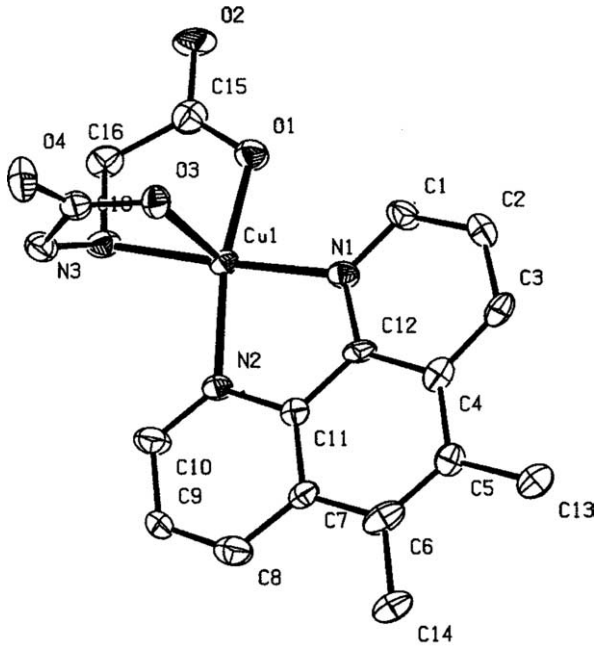

Fig. 2. ORTEP drawing of [Cu(imda)(5,6-dmp)] (**2**) showing the atom numbering scheme and the thermal motion ellipsoids (50% probability level) for the non-hydrogen atoms. Hydrogen atoms are omitted for clarity.

the other Cu–N_{phen} bond (2.045 Å), as it is *trans* to the weaker Cu–N_{amine} bond.

*3.1.1.3. [Cu(imda)(dpq)] (**3**).* The ORTEP view of the structure of **3** is shown in Fig. 3 and the selected bond lengths and bond angles are presented in Table 2. The asymmetric unit cell of the complex consists of two crystallographically independent molecules of the complex. Both the molecules have essentially identical coordination geometries, but the corresponding bond lengths and bond angles are slightly different. The geometry around copper(II) in each molecule is best described as trigonal bipyramidal distorted square-based pyramidal (TBDSBP) as revealed by the value of the structural index (τ) of 0.23, the corners of the CuN_3O square plane being occupied by two nitrogen atoms (N2, N3) of dpq, one of the carboxylate oxygen atoms (O3) and the tertiary amine nitrogen (N1) atom of the *cis*-facially coordinated imda anion. The axial position is occupied by the oxygen atom (O1) of the other carboxylate group of imda anion at a distance of 2.238 Å, longer than the equatorial O3 atom (Cu–O3, 1.935 Å) as a consequence of the presence of two electrons in d_{z^2} orbital. The Cu–N_{amine} bond (Cu–N1, 2.026 Å) is longer than the *trans* Cu–N_{dpq} bond [Cu–N3, 1.997 Å] formed by dpq, which is expected of sp^3 and sp^2 hybridizations, respectively, of amine and imine nitrogen atoms. Interestingly, the Cu–$N2_{dpq}$ bond (2.002 Å) is longer than the other Cu–N_{dpq} bond (1.997 Å), as it is *trans* to the stronger Cu–O3 bond. Also, one of the oxygen atoms (O4) of the carboxylate group from the neighboring molecule is located at the sixth position but at a distance of 2.889 Å with appreciable axial interaction with copper. Further, complex **3** displays a coordination structure very similar to **2** but with a higher τ value indicating that the coordination geometry of **3** is distorted towards trigonal bipyramidal more than **2**.

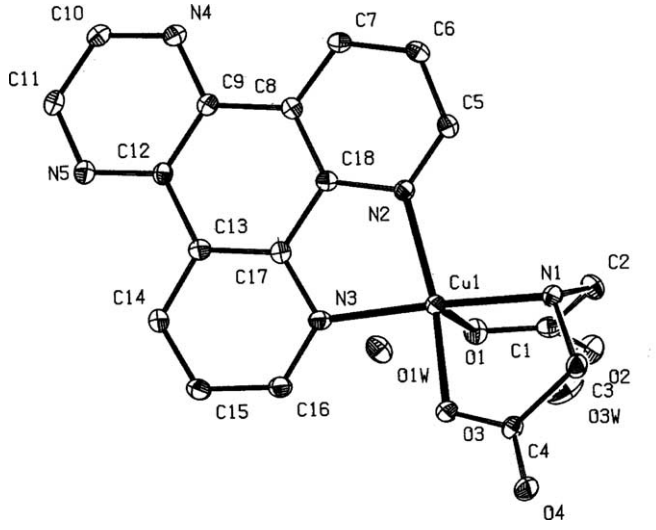

Fig. 3. ORTEP drawing of [Cu(imda)(dpq)] (**3**) showing the atom numbering scheme and the thermal motion ellipsoids (50% probability level) for the non-hydrogen atoms. Hydrogen atoms are omitted for clarity.

It is interesting to note that in all the complexes imda anion is involved in a *cis*-facial mode of coordination with one of the carboxylate oxygens axially coordinated at distances depending upon the diimine co-ligand located in the equatorial position: phen (2.313 Å) > 5,6-dmp (2.254 Å) > dpq (2.238 Å). This is in contrast the meridional coordination of the imda anion in [Cu(imda)(H_2O)$_2$] [42]. The possible rationale [38,43] for the observed preference for the equatorial positioning the $-COO^-$ groups in this complex is the shortest (1.962 Å) and hence the strongest bonds formed by the $-COO^-$ and secondary amines, defining the equatorial *xy*-plane, rather than one of them defaulting to a more weakly bound *z*-axial position as in the present complexes **1**–**3**. Thus, one of the strongly coordinating carboxylate oxygen atoms of imda anion in this complex is displaced from the equatorial plane to occupy the axial position because of the strong chelation of the diimines in the equatorial plane. Also, this is in contrast to the meridional coordination [44] of diethylenetriamine (dien) with stronger primary amino nitrogen atoms in [Cu(dien)(phen)]$^{2+}$, which, interestingly, leads to axial coordination of one of the phen ring nitrogen [Cu–N_{phen}(axial), 2.224 Å, Cu–N_{phen}(equatorial), 2.058 Å] and hence a higher trigonal constraint (τ, 0.31). Further, because of the strongly π-delocalized dpq, all the heterocyclic nitrogen atoms in **3** interact with copper(II) more strongly than those in **1**, this is consistent with the stronger axial interaction of the carboxylate oxygen atom of imda anion with copper as well as the enhanced constraint at copper (τ, 0.23) in **3**.

3.1.2. Spectral properties

In methanol:water (1:4 v/v) solution, all the complexes exhibit only one broadband in the visible region with very low molar absorptivity (Table 3), which is consistent with the square-based geometries in the solid-state structures (cf. above) and EPR spectral data (see below). The intense absorption band observed in the UV region (255–280 nm) is attributed to the intraligand $\pi \rightarrow \pi^*$ transitions of the coordinated COO^- group and diimines. A low intense band (345–368 nm), which is assignable to N(π) $\rightarrow$ Cu(II) LMCT transition (ε_{max}, 300–600 $M^{-1}\,cm^{-1}$), indicates the involvement of the imine nitrogen atoms in coordination even in solution. The frozen solution EPR spectra of the complexes are axial with $g_{\|} > g_{\perp} > 2.0$ and $G = [(g_{\|} - 2)/(g_{\perp} - 2)] = 3.6$ suggesting that the nearly square-based geometries observed in the solid state are retained in solution. Further, a square-based CuN_4 chromophore is expected [45,46] to show a $g_{\|}$ value of 2.200 and an $A_{\|}$ value of 180–200 $\times 10^{-4}\,cm^{-1}$ (Table 3) and the replacement of nitrogen atom in this chromophore by an oxygen atom is expected to increase the $g_{\|}$ value and decrease the $A_{\|}$ value. On the other hand, incorporation of strong axial interaction as in the present complexes would increase the $g_{\|}$ and decrease the $A_{\|}$ values. So the observed values of $g_{\|}$ (2.257) and $A_{\|}$ ($182 \times 10^{-4}\,cm^{-1}$) are consistent with the presence of a square-based CuN_3O chromophore involving

Table 3
Electronic[a], IR and EPR spectral properties of Cu(II) complexes

Complex	λ_{max} in nm (ε, $M^{-1}\,cm^{-1}$)			IR spectra			EPR spectra[d]	
	Ligand field[b]	Ligand based[c]	CT transition	ν_{as}	ν_s	$\Delta\nu$ (cm^{-1})		
[Cu(imda)(phen)(H_2O)] (**1**)	680 (50) 294 sh	273 (27,000)	345 (360)	1632	1385	247	$g_\parallel$ $A_\parallel$ $g_\perp$	2.257 180 2.066
[Cu(imda)(5,6-dmp)] (**2**)	680 (52) 303 sh	282 (26,350)	368 (463)	1634	1396	238	$g_\parallel$ $A_\parallel$ $g_\perp$	2.252 183 2.067
[Cu(imda)(dpq)] (**3**)	683 (51) 298 sh	258 (34,060)	354 (306)	1631	1388	243	$g_\parallel$ $A_\parallel$ $g_\perp$	2.253 180 2.076

[a] In methanol solution.
[b] Concentration 5×10^{-3} M.
[c] Concentration 2×10^{-5} M.
[d] Methanol/acetone glass at 77 K, $A_\parallel$ in $10^{-4}\,cm^{-1}$.

strong axial interaction, which is evident from the X-ray crystal structures.

3.1.3. Electrochemistry

In the cyclic voltammograms of all the three complexes in methanol solution obtained at 0.05 V s^{-1} scan rate, two cathodic peaks are observed (E^{I}_{pc}, −0.30 to −0.36; E^{II}_{pc}, −0.48 to −0.58 V, Table 4) and during the reverse scan an oxidation peak (E_{pa}, −0.064–0.20 V) is observed (Fig. 4). While the first reduction is due to $Cu^{II} \rightarrow Cu^{I}$ reduction of [Cu^{II}(imda)(phen)] species, the second reduction is due to the $Cu^{II} \rightarrow Cu^{I}$ process of [Cu^{II}(imda)] species (formed from the reaction of mixed-ligand Cu(II) species with mixed-ligand Cu(I) species, Scheme 1) observed more or less at the same potentials for all the present complexes and same as that observed for the reduction of [Cu^{II}(imda)] complex studied separately. While the Cu(II) oxidation state in [Cu^{II}(imda)] is stabilized by the strongly σ-bonding imda anion, the Cu(I) oxidation state in [Cu^{I}(diimine)$_2$]$^+$ is stabilized by the π-delocalized diimines. The reoxidation waves are located around potentials same as for [Cu(diimine)$_2$]$^{2+}$ complexes [47]. The Cu^{II}/Cu^{I} redox potentials of **1**–**3** depend upon the diimine co-ligand: dpq > phen > 5,6-dmp, reflecting the strong stabilization of Cu(I) oxidation state in [Cu^{I}(imda)(dpq)] by the extensive π-delocalization involving Cu(I) and dpq ligand more than phen and stabilization of Cu(II) oxida-

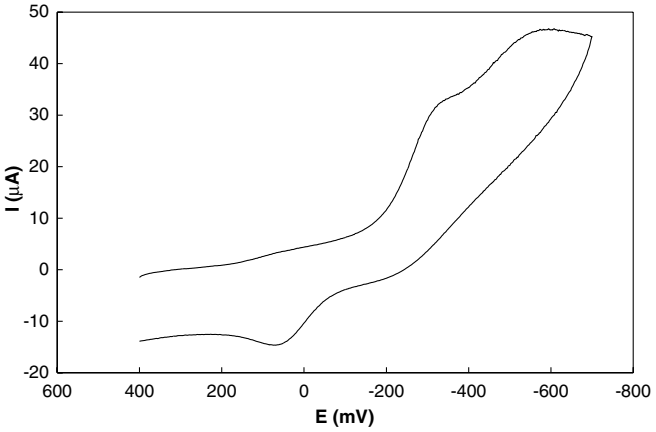

Fig. 4. Cyclic voltammograms of the complex **1** (1 mM) in methanol at 25 °C at 0.05 V s^{-1} scan rate.

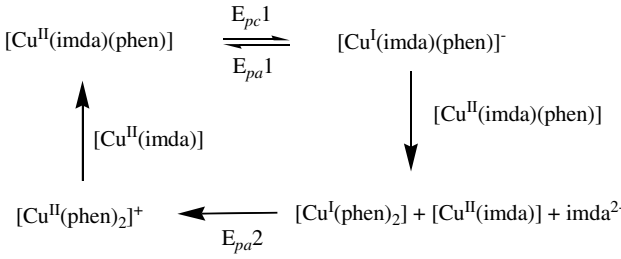

Scheme 1.

Table 4
Electrochemical data[a] for the copper(II) complexes at 25.0 ± 0.2 °C

Compound	E^{I}_{pc} (V)	E^{II}_{pc} (V)	E_{pa} (V)	$E_{1/2}$ (V)			$D \times 10^6$ ($cm^2\,s^{-1}$)
				DPV[Ib]	DPV[II]	DPV[III]	
[Cu(imda)(phen)(H_2O)] (**1**)	−0.336	−0.574	0.068	0.093	−0.287	−0.565	2.5
[Cu(imda)(5,6-dmp)] (**2**)	−0.354	−0.576	0.064	0.055	−0.395	−0.539	9.0
[Cu(imda)(dpq)] (**3**)	−0.318	−0.486	0.200	0.175	−0.265	−0.495	1.7

[a] Measured vs. non-aqueous Ag/Ag^+ reference electrode; add 544 mV [300 mV, Ag/Ag^+ to SCE + 244 mV, SCE to SHE] to convert to standard hydrogen electrode (SHE); Fc/Fc^+ couple, $E_{1/2}$, 0.039 V (CV); 0.042 (DPV), scan rate 50 mV s^{-1}; Supporting electrolyte, *Tetra-N*-butylammonium perchlorate (0.1 mol dm^{-3}); Complex concentration, 1 mmol dm^{-3}.
[b] Differential pulse voltammetry, scan rate 2 mV s^{-1}; pulse height 50 mV.

tion state by the electron-repelling methyl groups in 5,6-dmp more than phen diimines.

3.2. DNA-binding studies

3.2.1. Absorption spectral studies

On the addition of CT DNA all the complexes show a decrease in molar absorptivity (hypochromism, 40–60%, Fig. 5A) of the $\pi \rightarrow \pi^*$ absorption band indicating strong binding of the complexes to DNA. These changes are typical of a complex bound to DNA through intercalation involving insertion of the aromatic chromophore of the diimine ligands in between the base pairs of DNA. As the extent of hypochromism is commonly consistent with the strength of intercalative interaction [48–50], the observed trend in hypochromism, **3** > **2** > **1** reflects the trend in DNA-binding affinities of the complexes. From the observed spectral changes the value of the intrinsic equilibrium DNA-binding constant K_b was determined by regression analysis using Eq. (1) (Fig. 5B) [51,52], which includes binding site size:

$$(\varepsilon_a - \varepsilon_b)/(\varepsilon_b - \varepsilon_f) = (b - (b^2 - 2K_b^2 C_t[\mathrm{DNA}]/s)^{1/2})/2K_b C_t, \quad (1a)$$

$$b = 1 + K_b C_t + K_b[\mathrm{DNA}]/2s, \quad (1b)$$

where ε_a is the extinction coefficient observed for the MLCT absorption band at a given DNA concentration, ε_f is the extinction coefficient of the complex free in solution, ε_b is the extinction coefficient of the complex when fully bound to DNA, K_b is the equilibrium binding constant, C_t is the total metal complex concentration, [DNA] is the DNA concentration in nucleotides, and s is the binding site size in base pairs. Eq. (1) has been applied to absorption and emission titration data assuming non-cooperative metallointercalator binding to calf-thymus (CT) DNA [53]. The value of K_b obtained (Table 5) follows the order **3** > **2** > **1**, which is in conformity with the observed trend in hypochromism. The K_b value of the dpq complex is much higher than the phen analogue, which is expected of the extended aromatic ring of dpq inserted in between the base stack of DNA more deeply than the phen analogue [54]. Further, the introduction of methyl groups on the phen ring at 5,6-positions may appear to hinder the partial intercalation of the phen ring; however, a strong hydrophobic interaction between 5,6-dmp ligand and the hydrophobic interior accessible in DNA [55] is plausible.

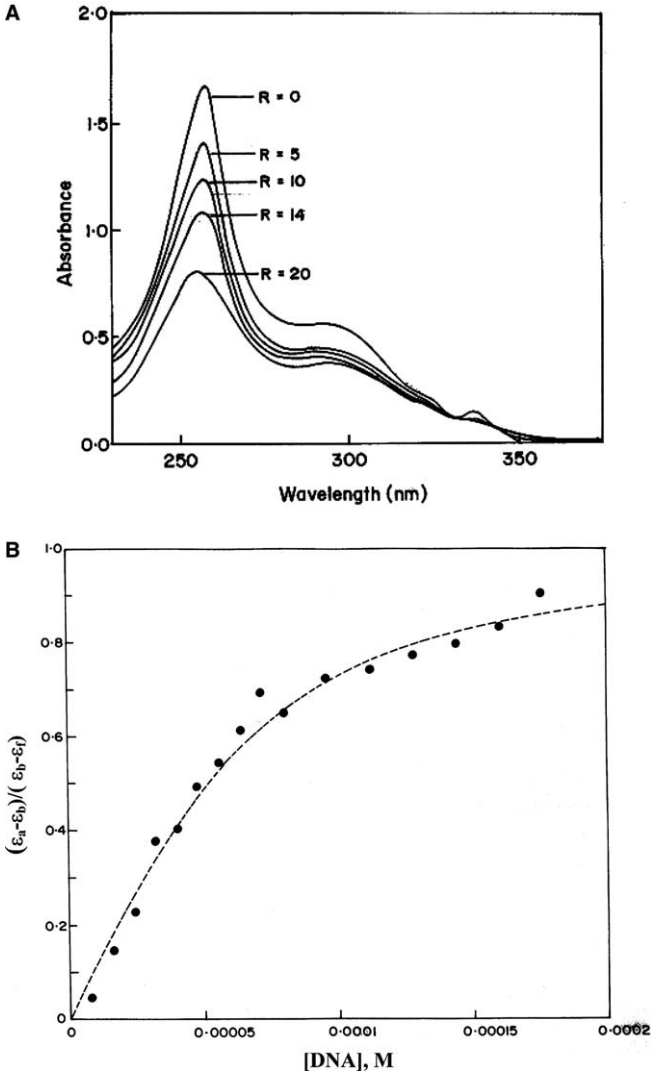

Fig. 5. (A) Absorption spectra of [Cu(imda)(dpq)] (1.7×10^{-5} M) in 5 mM Tris–HCl buffer at pH 7.1, in the absence ($R = 0$) and presence ($R = 5$, 10, 14, 20, 25) of increasing amounts of DNA. (B) Plot of $(\varepsilon_a - \varepsilon_b)/(\varepsilon_b - \varepsilon_f)$ vs. [DNA] for [Cu(imda)(dpq)]. The best fit line, superimposed on the data, according to Eqs. (1a) and (1b) yields $K_b = 1.7 \times 10^4$ M^{-1} and $s = 0.16$.

Table 5
Absorption spectral properties of Cu(II) complexes bound[a] to CT DNA and difference in DNA melting temperatures on interactions with copper(II) complexes[b]

Complex	Ligand-based							
	λ_{max} (nm)	R	Change in absorbance	$\Delta\varepsilon$ (%)	Redshift (nm)	$K_b \times 10^3$ (M^{-1})	s[c]	ΔT_m (°C)
[Cu(imda)(phen)(H_2O)] (**1**)	273	25	Hypochromism	41	0	0.60 ± 0.04	0.05	5.70 ± 0.05
[Cu(imda)(5,6-dmp)] (**2**)	282	25	Hypochromism	52	2	3.90 ± 0.30	0.09	5.50 ± 1.0
[Cu(imda)(dpq)] (**3**)	258	25	Hypochromism	63	1	17.0 ± 5.0	0.16	10.6 ± 1.0

[a] Measurements were made at $R = 25$, where R = [DNA]/[Cu complex], concentration of copper(II) complex solutions = 2.8×10^{-5} M (**1**), 3.0×10^{-5} M (**2**) and 8×10^{-6} (**3**).
[b] Measurements were made at R value of 0.1.
[c] Binding site size in base pairs.

A similar observation has been made for [Ru(5,6-dmp)-$(NH_3)_4]^{2+}$, which interacts more strongly than [Ru(phen)-$(NH_3)_4]^{2+}$ due to the strong hydrophobic interaction between 5,6-dmp ligand and the hydrophobic interior accessible in DNA [55]. It is interesting that the present complexes, in spite of their being neutral with no potential to engage in electrostatic interaction, exhibit strong DNA-binding affinities due to possible hydrogen bonding interactions between coordinated –NH– and two carboxylate oxygens with the functional groups positioned in the edge of the DNA bases [55]. Similar hydrogen bonding interactions have been proposed for $[Co(NH_3)_6]^{3+}$ bound to $d(CG)_3$ [56] and $[Ru(diimine)(NH_3)_4]^{2+}$ [57] bound to CT DNA.

3.2.2. Viscosity and thermal denaturation studies

The values of relative specific viscosity (η/η_0), where η and η_0 are the specific viscosities of DNA in the presence and absence of the complex, are plotted against $1/R$ (= [Cu complex]/[NP] = 0.05–0.5) (Fig. 6). The significant increase in viscosity of the dpq complex, which, however, is less than that for the potential intercalator viz., ethidium bromide [58], is obviously due to the partial insertion of the dpq ligand in between the DNA base pairs (cf. above) leading to increase in separation of base pairs at intercalation sites and hence an increase in overall DNA contour length [59,60,30]. As expected, the phen complex involved in partial intercalative DNA binding less strongly than the dpq complex displays a lower increase in DNA viscosity. The interesting decrease in viscosity observed for the 5,6-dmp complex suggests that the hydrophobic interaction of the 5,6-dmp ligand with DNA surface, encouraged by the stronger hydrogen bonding interactions, leads to bending (kinking) of the DNA chain. In fact, we have observed a similar bending of DNA on covalent binding of copper(II) complexes of certain tridentate 3N ligands [30]. It is also possible that the complex stabilizes the A form DNA helix (cf. below), which is shorter and fatter than the B form DNA. The DNA melting curves obtained in the presence of DNA reveal a monophasic and irreversible melting of the DNA strands. The dpq complex 3 shows a ΔT_m value of 10 ± 1 °C (Table 5), which is typical of intercalating metal complexes ($10–14 \pm 1$ °C) [61]. The partial insertion of the planar aromatic dpq ligand in between the DNA base pairs causes stabilization of base stack and hence raises the melting temperature of the double-stranded DNA [62]. On the other hand, Complexes **1** and **2** show lower ΔT_m values ($5–6 \pm 1$ °C) indicative of their non-intercalative DNA binding.

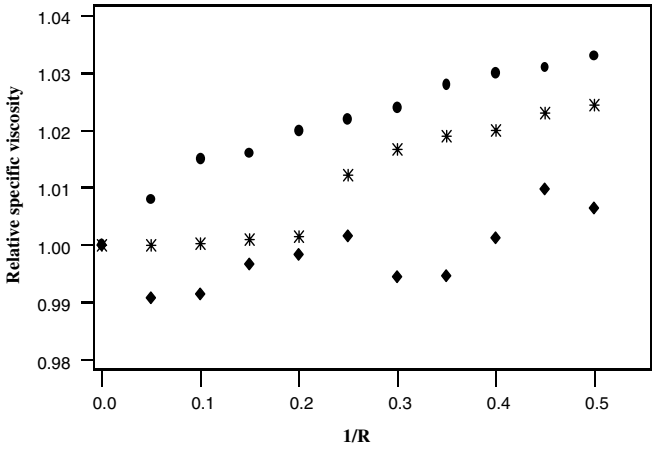

Fig. 6. The effect of [[Cu(imda)(phen)(H_2O)] (✳), [Cu(imda)(dmp)] (♦), [Cu(imda)(dpq)] (●) on the viscosity of CT DNA; Relative specific viscosity vs. $1/R$; [CT DNA] = 500 μM.

3.2.3. Circular dichroism

The observed CD spectrum of calf-thymus (CT) DNA consists of a positive band at 275 nm (UV; λ_{max}, 258 nm) due to base stacking and a negative band at 245 nm due to helicity, which are characteristic of DNA in right-handed B form [63]. When the present complexes are incubated with CT DNA at $1/R$ (= [Cu complex]/[DNA]) values of **1** and **3**, the CD spectrum of DNA undergoes changes in both positive and negative bands (Table 6 and Fig. 7A and C) consistent with the partial intercalative interaction of **1** and **3**. Also, a high intensity band due to induced CD (ICD) is located at 278, 290 and 268 nm (which are the positions of the UV absorption bands of the complexes) respectively for **1**, **2** and **3** on the broad positive band. The large decrease in intensity of the DNA helicity band with a higher red-shift observed for **2** (Fig. 7B) indicates that the complex exhibits a mode of DNA binding different from **1** and **3**. It is possible that upon interaction with **2** the B-DNA transforms into an A-like conformation [64,65]. The shift in the positive ellipticity band from 274 to 290 nm supports this type of transformation. It is proposed that the two 5,6-methyl groups of **2** act to effectively place the complex in the major groove leading to the conversion of B to A DNA, which has a major groove to accommodate complex. When the ionic strength of the buffer is increased from 0.05 to 1 M [NaCl] keeping the mixing ratio constant ($1/R = 2$ for **1** and **2**; 1 for **3**), the ICD, interestingly, disappears for all the complexes and the original CD spectrum corresponding to B conformation is obtained at 1 M NaCl for **1** and **2** and at a higher concentration for **3** (Figure S1). This reveals that the binding of the complexes is reversible with Na^+ ion being effective in displacing the DNA-bound complexes.

Table 6
CD parameters for the interaction of calf-thymus DNA with copper(II) complexes

Sample	CD spectral band[a]	
	Wavelength (nm)	
CT DNA	245	277
[Cu(imda)(phen)(H_2O)] (**1**)	249	279
[Cu(imda)(5,6-dmp)] (**2**)	252	291
[Cu(imda)(dpq)] (**3**)	244	268

[a] Measurement made at $1/R$ value of 2 for complexes **1** and **2** and 1 for complex **3**, where $1/R$ = [Cu]/[NP]; concentration of DNA solutions = 2.5×10^{-5} M. Cell path length = 1 cm.

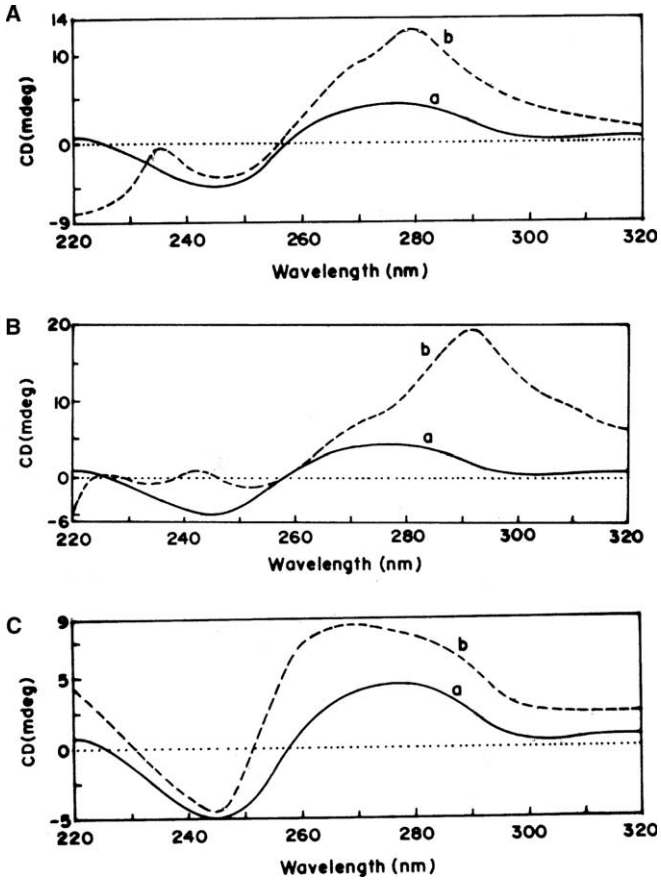

Fig. 7. (A) Circular dichroism spectra of CT DNA in the absence (a) and presence (b) of [Cu(imda)(phen)(H_2O)] at $1/R$ value of 2. (B) Circular dichroism spectra of CT DNA in the absence (a) and presence (b) of [Cu(imda)(5,6-dmp)] at $1/R$ value of 2. (C) Circular dichroism spectra of CT DNA in the absence (a) and presence (b) of [Cu(imda)(dpq)] at $1/R$ value of 2; [CT DNA] $= 2 \times 10^{-5}$ M.

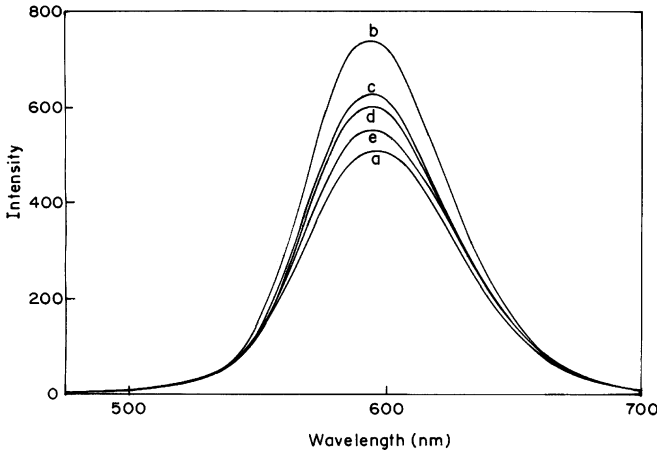

Fig. 8. Emission spectra of ethidium bromide in the absence (a) and presence of CT DNA, (b) DNA + [Cu(imda)(phen)(H_2O)], (c) DNA + [Cu(imda)(dpq)], (d) DNA + [Cu(imda)(5,6-dmp)] and (e) [complex], [EthBr], [DNA] $= 1 \times 10^{-5}$ M.

Thus, complex **2** is involved in groove binding while **1** and **3** are involved in partial intercalation with CT DNA.

3.2.4. Competitive DNA-binding studies

In competitive ethidium bromide (EthBr) binding studies, the complexes **1**–**3** were added to DNA pretreated with EthBr ([DNA]/[EthBr] = 1) and then emission intensities of DNA-induced EthBr [57] were measured (Fig. 8). Addition of a second DNA-binding molecule would quench the EthBr emission by either replacing DNA-bound EthBr (if it binds to DNA more strongly than EthBr) and/or by accepting the excited state electron from EthBr. As the present diimine complexes are not expected to efficiently compete with the strong intercalator EthBr for the intercalative binding sites, the EthBr displacement mechanism is ruled out. If the quenching occurs by photoelectron transfer mechanism, then the ability of the complexes to quench the EthBr emission intensity should vary as **3** > **1** > **2**, depending upon the reducibility of the copper(II) complexes (cf. above). However, the observed ability of the imda complexes to hinder the DNA induced enhancement in EthBr emission decreases in the order, **2** (73%) > **3** (60%) > **1** (49%). It is interesting that the 5,6-dmp complex, which is shown by viscosity measurements not to involve in intercalative interaction with DNA, hinders the enhancement in emission of EthBr much better than the dpq complex, in spite of its more negative Cu(II)/Cu(I) redox potential. Obviously, the more rigid and shorter A-like conformation of DNA, stabilized by the 5,6-dmp complex through hydrophobic interaction in DNA grooves, is either not suitable for intercalative interaction by EthBr leading to its displacement or destabilizes the excited state of bound EthBr and hence the latter is displaced.

3.3. Nuclease activity of complexes and mechanistic investigations

3.3.1. Oxidative cleavage of DNA

The ability of the complexes in effecting DNA cleavage has been investigated by gel electrophoresis using supercoiled pBR322 DNA in 5 mM Tris–HCl/50 mM NaCl buffer solution (pH 7.1). For comparison cleavage reactions were carried out also with $[Cu(diimine)]^{+}$ and $[Cu(diimine)_2]^{2+}$ complexes (diimine = phen, 5,6-dmp and dpq). All the complexes are found to exhibit nuclease activity (Fig. 9A and Table 7). Control experiments using only ascorbic acid (H_2A) do not show any apparent cleavage of DNA (lane 1). The cleavage efficiency of **1**–**3** (lanes 2–4) in the presence of ascorbic acid is close to those exhibited by the corresponding mono- and bis-diimine complexes. Based upon their ability to convert supercoiled form (Form I, SC) to nicked circular (Form II, NC) and then to linear open circular DNA (Form III, LC), the propensity of the complexes to fully convert the SC to NC and then to LC form varies as **3** (NC 70%, LC 30%, lane 5) > **1** (NC 53%, lane 3) ≅ **2** (NC 51%, lane 4). In contrast to **3** the bis-complex $[Cu(dpq)_2]^{2+}$ effects SC to NC (87%) and then NC to only LC form (13%) thus revealing that **3** behaves as an efficient chemical nuclease for double-strand cleavage of

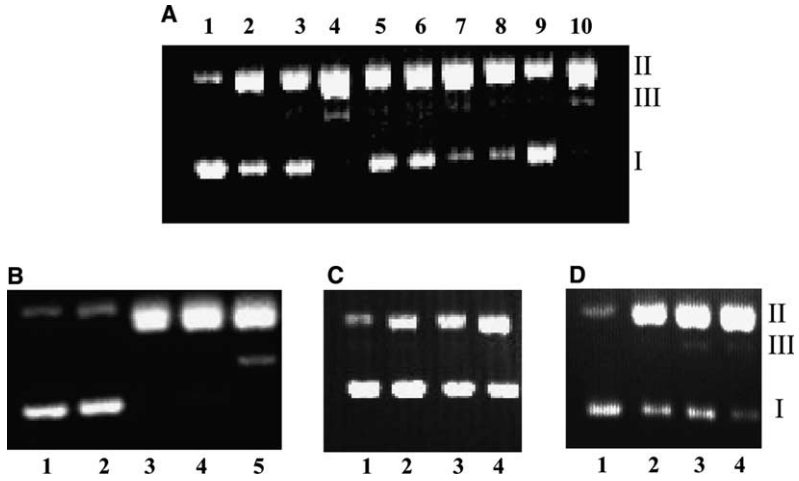

Fig. 9. (A) Cleavage of supercoiled pBR322 DNA (10 μM) by the copper(II) complexes in a buffer containing 50 mM Tris–HCl and 50 mM NaCl in the presence of ascorbic acid (H_2A, 10 μM) at 37 °C. Lane 1, DNA + H_2A; lane 2, DNA + [Cu(imda)(phen)(H_2O)] + H_2A; lane 3, DNA + [Cu(imda)(5,6-dmp)] + H_2A; lane 4, DNA + [Cu(imda)(dpq)] + H_2A; lane 5, DNA + [Cu(phen)] + H_2A; lane 6, DNA + [Cu(5,6-dmp)] + H_2A; lane 7, DNA + [Cu(dpq)] + H_2A; lane 8, DNA + $[Cu(phen)_2]^{2+}$ + H_2A; lane 9, $[Cu(5,6\text{-dmp})_2]^{2+}$ + H_2A; DNA + $[Cu(dpq)_2]^{2+}$ + H_2A . Complex concentration is 30 μM for lanes 2–10. Forms I, II and III are supercoiled, nicked circular and linear forms of DNA, respectively. (B) Lane 1, DNA; lane 2, DNA + ethanol + H_2A; lane 3, DNA + [Cu(imda)(phen)(H_2O)] + H_2A + ethanol; lane 4, DNA + [Cu(imda)(5,6-dmp)] + H_2A + ethanol; lane 5, DNA + [Cu(imda)(dpq)] + H_2A + ethanol. Complex, ethanol concentration is 30 μM and 1 M for lanes 2–5. (C) Lane 1, DNA + H_2A + NaN_3; lane 2, DNA + [Cu(imda)(phen)-(H_2O)] + H_2A + NaN_3; lane 3, DNA + [Cu(imda)(5,6-dmp)] + H_2A + NaN_3; lane 4, DNA + [Cu(imda)(dpq)] + H_2A + NaN_3. Complex, NaN_3 concentration is 30 μM and 100 mM for lanes 1–4. (D) Lane 1, DNA + H_2A + distamycin, lane 2, DNA + [Cu(imda)(phen)(H_2O)] + H_2A + distamycin; lane 3, DNA + [Cu(imda)(5,6-dmp)] + H_2A + distamycin; lane 4, DNA + [Cu(imda)(dpq)] + H_2A + distamycin. Complex, distamycin concentration is 30 μM and 100 μM for lanes 1–4.

Table 7
Comparison of the pBR322 DNA cleavage efficiency of complexes **1**–**3** along with six reference copper(II) complexes in the presence of ascorbic acid (H_2A)

Serial no.	Reaction condition	Form (%)		
		SC	NC	LC
Fig. 8A				
1	DNA + H_2A	63	37	
2	DNA + H_2A + [Cu(phen)(imda)(H_2O)] (**1**)	47	53	
3	DNA + H_2A + [Cu(5,6-dmp)(imda)] (**2**)	49	51	
4	DNA + H_2A + [Cu(dpq)(imda)] (**3**)		70	30
5	DNA + H_2A + [Cu(phen)(H_2O)]Cl_2	49	51	
6	DNA + H_2A + [Cu(5,6-dmp)(H_2O)]Cl_2	47	53	
7	DNA + H_2A + [Cu(dpq)(H_2O)]Cl_2	32	68	
8	DNA + H_2A + $[Cu(phen)_2(H_2O)Cl_2]$	35	65	
9	DNA + H_2A + $[Cu(5,6\text{-dmp})_2(H_2O)Cl_2]$	57	43	
10	DNA + H_2A + $[Cu(dpq)_2(H_2O)Cl_2]$		87	13

DNA much better than both $[Cu(dpq)]^{2+}$ and $[Cu(dpq)_2]^{2+}$. The intense nuclease activity of **3** is apparently due to the enhanced stabilization of the Cu(I) species $[Cu(imda)(dpq)]^{-}$, as evidenced by its highest Cu(II)/Cu(I) redox potential through increased π-delocalization involving quinoxaline moiety of dpq and Cu(I). Further, its ability to effect a second scission on the complementary strand, within about 12 base pairs from the first one [11], to generate the linear DNA form may be attributed to its ability to intercalate into the DNA helix and remain bound at the nick site after nicking for reactivation and complementary strand cleavage [66]. The presence of the DNA-bound complexes close to the deoxyl ribose rings [67] is possibly supported by the hydrogen bonding interactions of imda co-ligand through –NH– and carboxylate oxygens, as understood from spectral properties.

On adding ethanol (hydroxy radical scavenger) no inhibition of DNA cleavage is observed indicating that hydroxyl radical is not involved in the cleavage process (Fig. 9B). On the other hand, addition of sodium azide (singlet oxygen scavenger) decreases the cleavage efficiencies but slightly (Fig. 9C); this reveals that $^1O_2$ is not the activated oxygen intermediate responsible for the cleavage. The slight suppression of cleavage may be ascribed to the affinity of sodium azide for transition metals [68]. Addition of superoxide dismutase (superoxide scavenger) to the reaction mixture show no significant quenching of the cleavage reaction revealing that superoxide anion is not also the active species (not shown) [68]. Thus no freely diffusible oxygen intermediate or hydroxyl radical is involved in the strand scission and hence a simple diffusible radical mechanism is ruled out. This led us to propose that the active

species is most possibly copper-oxene or a copper-coordinated hydroxyl radical, which is directly responsible for initiating the cleavage reaction [69,70]. The reactive species remains tightly coordinated to copper(II), thus preventing them from being deactivated by radical inhibitors. A 'copper-oxene' or a resonance hybrid of a copper(II)-hydroxyl radical and a putative copper(III)-oxo species, which generates a deoxyribose-centered radical by C-1 hydrogen abstraction, is the species responsible for DNA cleavage [69,70].

When pBR322 DNA was treated with distamycin, a minor groove binder, the cleavage reaction mediated by **1** and **2** was not quenched. This clearly suggests that the complexes prefer to bind to DNA major groove. However, for **3** the extent of scission was up to NC, the LC form disappear (Fig. 9D) and the slight quenching of cleavage reaction reveals that the complex prefers to bind to the minor groove [71] unlike the phen and 5,6-dmp analogues. Further, on treating $[Cu(dpq)_2]^{2+}$ with ascorbic acid a diamagnetic blue species of $[Cu(dpq)_2]^{+}$ was instantaneously precipitated [47]. On the other hand, treatment of [Cu(dpq)(imda)]$^{2+}$ with ascorbic acid yielded no blue species suggesting that [Cu(dpq)(imda)]$^{+}$ rather than the $[Cu^{I}(dpq)_2]^{+}$ species is the complex species involved in cleavage. Similarly, complexes **1** and **2** show a trend in cleavage similar to their 1:1 complexes [Cu(phen)]$^{2+}$ and [Cu(5,6-dmp)]$^{2+}$. It has been postulated earlier that [Cu(diimine)]$^{2+}$ complexes bind at the minor groove of B-DNA and generates freely diffusible hydroxyl radical, which abstracts C1 hydrogen [72]. As hydroxyl radicals are found to be not involved in the cleavage, the possibility of formation of [Cu(diimine)]$^{+}$ is ruled out. Further, the efficiency of **3** to cleave double-stranded DNA is higher than those for $[Cu(dpq)_2]^{2+}$ and [Cu(dpq)]$^{2+}$.

3.3.2. Hydrolytic cleavage of DNA

Interestingly, complexes **1**–**3** are found to hydrolytically cleave DNA in the absence of any reducing agent or light (Table 8). At a concentration of 0.5 mM and an incubation time of 3 h, the phen and dpq complexes exhibit complete cleavage while the 5,6-dmp complex cleaves only 60% of SC-DNA (Fig. 10A). Also, interestingly, the dpq complex **3** effects SC to NC (72%) and then NC to LC form (28%) thus revealing that it behaves as an efficient chemical nuclease for double-strand cleavage of DNA much better than both **1** and **2**. The complex $[Cu(imda)(H_2O)_2]$ does not show any significant cleavage activity under similar conditions. The gel diagram showing the extent of DNA

Table 8
Hydrolytic cleavage of DNA (SC pBR322, 12 μM) by complexes **1**–**3** (0.5 mM) in the absence of any reducing agent for an incubation time 3 h

Serial no.	Reaction conditions	Form (%)		
		SC	NC	LC
Fig. 9A				
1	DNA control	95	5	
2	DNA + **1**	4	96	
3	DNA + **2**	40	60	
4	DNA + **3**		72	28
5	DNA + $[Cu(imda)(H_2O)_2]$	80	20	
6	DNA + **1**	10	90	
7	DNA + **2**	32	68	
8	DNA + **3**		78	22
9	DNA + DMSO + **3**	85	15	

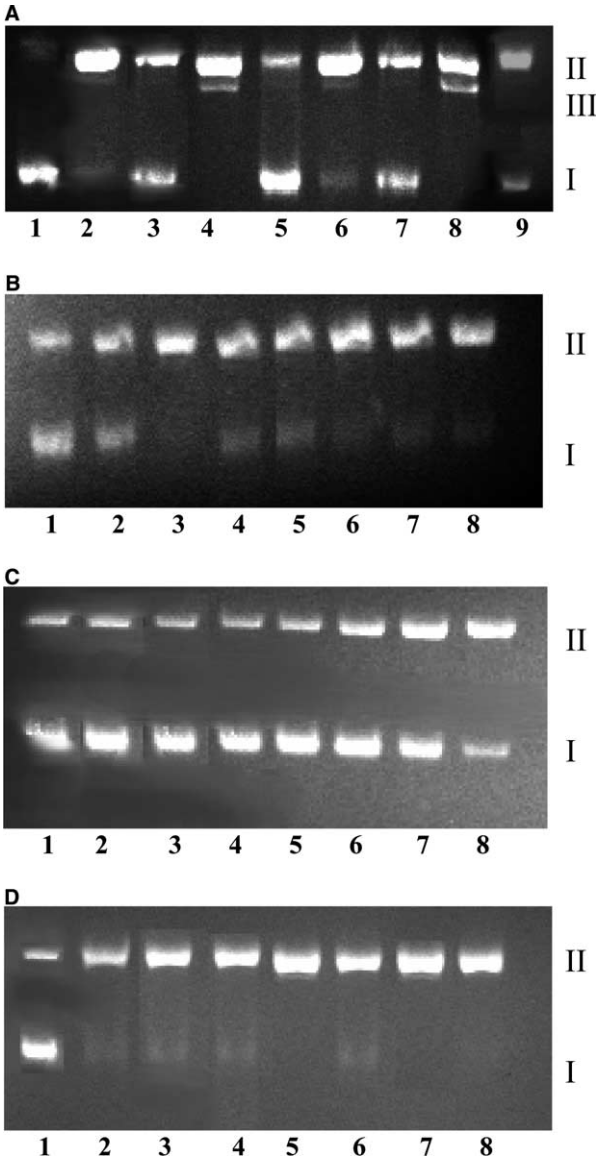

Fig. 10. (A) Gel electrophoresis diagram showing the hydrolytic cleavage of supercoiled pBR322 DNA (12 μM) by complexes **1**–**3** (0.5 mM) under aerobic for lanes 1–4 and anaerobic for lanes 5–8 and with an incubation time of 3 h in 10 mM HEPES buffer: lane 1, DNA control; lane 2, DNA + **1**; lane 3, DNA + **2**; lane 4, DNA + **3**; lane 5, DNA + [Cu(imda)$(H_2O)_2$]; lane 6, DNA + **1;** lane 7, DNA + **2**; lane 8, DNA + **3**; lane 9, DNA + DMSO + **3**. (B) Time course of pBR322 DNA (12 μM) cleavage by complex **1**: 0.5 mM at pH 8.1 (10 mM HEPES) and 37 °C incubation times are 0, 10, 30, 50, 60, 80, 100, 120 min for lanes 1–8. (C) Time course of pBR322 DNA (12 μM) cleavage by complex **2**: 0.5 mM at pH 8.1 (10 mM HEPES) and 37 °C incubation times are 0, 10, 30, 50, 60, 80, 100, 120 min for lanes 1–8. (D) Time course of pBR322 DNA (12 μM) cleavage by complex **3**: 0.5 mM at pH 8.1 (10 mM HEPES) and 37 °C incubation times are 0, 10, 30, 50, 60, 80, 100, 120 min for lanes 1–8.

cleavage by the complexes **1**–**3** with reaction time is displayed in Fig. 10B, C and D. Both the decrease in form I (SC) and formation of form II (NC) of DNA with time are exponential as expected. The plots of log (% SC-DNA) with time gave linear fits (Fig. 11) from which the hydrolytic pseudo-first-order rate constant ($k_{obsd.}$) are

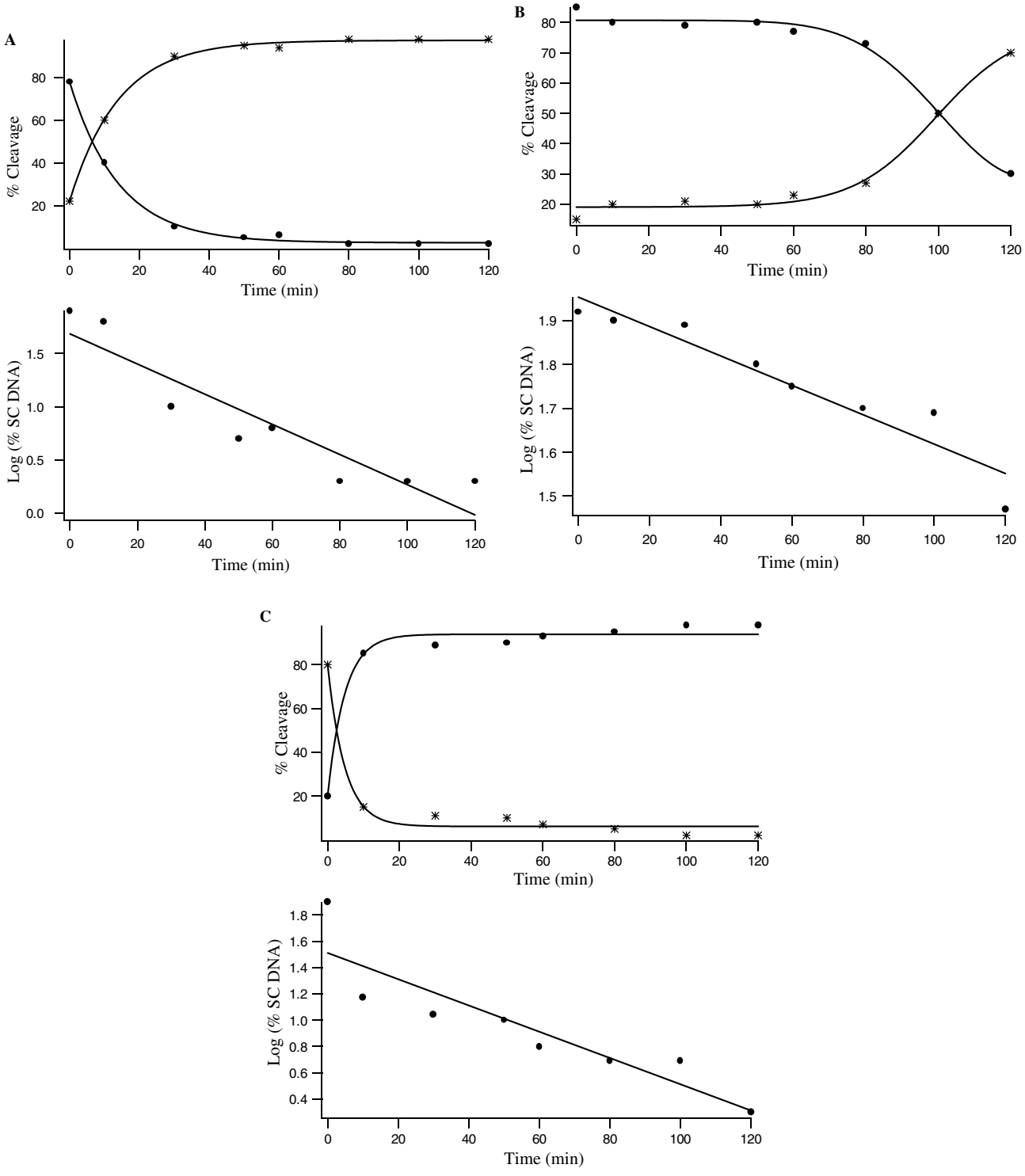

Fig. 11. (A) Hydrolytic cleavage of supercoiled pBR322 DNA (12 μM) showing the decrease in form I (SC-DNA) and the formation of form II (NC DNA) with the incubation time using 0.5 mM concentration of **1**; the plot shows of log (% SC-DNA) vs. time for complex **1** (0.5 mM) at 37 °C at pH 8.1 (10 mM HEPES) for an incubation period of 0–120 min. (B) Hydrolytic cleavage of supercoiled pBR322 DNA (12 μM) showing the decrease in form I (SC DNA) and the formation of form II (NC DNA) with the incubation time using 0.5 mM concentration of **2**; the plot shows log (% SC-DNA) vs. time for complex **2** (0.5 mM) at 37 °C at pH 8.1 (10 mM HEPES) for an incubation period of 0–120 min. (C) Hydrolytic cleavage of supercoiled pBR322 DNA (12 μM) showing the decrease in form I (SC-DNA) and the formation of form II (NC DNA) with the incubation time using 0.5 mM concentration of **3**; the plot shows log (% SC-DNA) vs. time for complex **3** (0.5 mM) at 37 °C at pH 8.1 (10 mM HEPES) for an incubation period of 0–120 min.

obtained (**1**, 0.85, **2**, 0.20, **3**, or 0.60 h^{-1}) using a complex concentration of 0.5 mM. The rate of hydrolytic cleavage by **1** is faster than **2** and **3** and is greater than that by copper(II)-L-histidine complex (0.76 h^{-1} at 1 mM conc. of the complex) [73]. The cleavage reactions were observed even in the presence of dinitrogen ruling out the possibility of an oxidative cleavage pathway. The commonly accepted mechanism of hydrolysis of deoxynucleotide phosphates involves a nucleophilic attack of a water oxygen to the phosphorus to give a five co-ordinate phosphate intermediate [21,74]. In the present complexes, the higher rate of hydrolysis observed for the complex **1** may be traced to the presence of axially coordinated water molecule, which may be activated as a nucleophile for the hydrolytic cleavage [75,76]. Complexes **2** and **3** with no water of coordination in the solid state (due to stronger coordination of axial carboxylate oxygen, see above) may become coordinated but weaker than **3** in solution and hence have a lower potential to activate coordinated water molecule as a nucleophile. Interestingly, no significant cleavage was observed for the complex [Cu(imda)(H_2O)$_2$] with equatorial coordination of carboxylate oxygen of imda anion. So it is clear that the axially coordinated carboxylate of imda anion promotes and regulates the Lewis acid/base activity needed for the hydrolytic cleavage. Further, the primary role of the bidentate diimine ligand is to facilitate the axial coordination of the carboxylate oxygen of imda anion (cf above), in addition to deciding groove selectivity [77].

4. Conclusions

Three new mixed ligand copper(II) complexes of the type [Cu(imda)(diimine)], where H_2imda is iminodiacetic acid and diimine is 1,10-phenanthroline or 5,6-dimethyl-1,10-phenanthroline or dipyridoquinoxaline, have been isolated and their X-ray crystal structures determined. While [Cu(imda)(phen)(H_2O)] possesses a distorted octahedral coordination geometry, [Cu(imda)(5,6-dmp)] and [Cu(imda)(dpq)] possess trigonal bipyramidal distorted square-pyramidal (TBDSBP) geometries. Interestingly, in all these complexes the imda anions are *cis*-facially coordinated in contrast to its meridional coordination in [Cu(imda)(H_2O)$_2$]. The square-based geometries of the complexes are preserved in aqueous buffer solution as diagnosed by the ligand-field and axial EPR spectra. The DNA binding of the complexes involve partial intercalation of phen and dpq and the hydrophobic interaction of 5,6-dmp with DNA. Viscosity and thermal denaturation studies reveal that the dpq complex interacts through partial intercalation of dpq through its extended aromatic chromophore more strongly than the phen complex. The [Cu(5,6-dmp)(imda)] complex shows a decrease in relative viscosity, which is characteristic of bending or kinking of DNA and/or stabilization of the shorter and compact A-like DNA conformation. Also it facilitates the quenching of the DNA-induced ethidium bromide emission much better than other complexes by stabilizing the A form of DNA. The oxidative DNA cleavage studies show that the dpq complex is bound in the DNA minor groove while the phen and 5,6-dmp complexes are bound in the DNA major groove. As the mixed ligand dpq complex shows a unique ability to effect DNA double-strand scission in both the oxidative and hydrolytic cleavage reactions, it is proposed as a new and better DNA-binding and DNA-cleaving agent and hence as an artificial restriction enzyme in nucleic acid chemistry.

5. Abbreviations

CD	circular dichroism
CT DNA	calf-thymus DNA
DMSO	dimethyl sulfoxide
DPPH	diphenylpicrylhydrazyl
EDTA	ethylenediamine-*N*,*N*,*N*′,*N*′-tetraacetate
EthBr	ethidium bromide
HEPES	4-(2-hydroxyethyl)-1-piperazineethanesulfonic acid
MLCT	metal-to-ligand charge transfer
TAE	tris acetate EDTA
Tris	tris-(hydroxymethyl) aminomethane

Acknowledgments

Council of Scientific and Industrial Research, New Delhi (Grant No. 01(1693)/01/EMR-II) and Department of Atomic Energy, Mumbai, India (Grant No. 2003/37/25/BRNS) are gratefully acknowledge for financial support. We thank Dr. K.V. Krishnamurthy, Bharathidasan University and Dr. P. Sambasiva Rao, Pondicherry University, Pondicherry for providing the Gel Documentation and EPR facilities, respectively. University Grants Commission (UGC), New Delhi and DST, New Delhi are greatly acknowledged for funding to generate Instruments Facility in the Department through Special Assistance Program (SAP) of UGC and Funds for Improvement of S&T Infrastructure (DST-FIST) program of Department of Science and Technology, New Delhi, respectively.

Appendix A. Supplementary data

X-ray crystallographic data for **1**, **2** and **3** in CIF format and CD Figure (Figure S1). Supplementary data associated with this article can be found, in the online version, at doi:10.1016/j.jinorgbio.2005.11.018.

References

[1] C.J. Burrows, S.E. Rokita, Acc. Chem. Res. 27 (1994) 295–301.
[2] A.M. Pyle, J.K. Barton, S.J. Lippard (Eds.), Progress in Inorganic Chemistry, vol. 38, Wiley, New York, 1990, p. 413.
[3] T.D. Tullius, Metal-DNA ChemistryACS Symposium Series, vol. 402, American Chemical Society, Washington, DC, 1989.

[4] A.R. Banerjee, J.A. Jaeger, D.H. Turner, Biochemistry 32 (1993) 153–163.
[5] G. Pratviel, J. Bernadou, B. Meunier, Angew. Chem., Int. Ed. Engl. 34 (1995) 746–769.
[6] D.S. Sigman, Biochemistry 29 (1990) 9097–9105.
[7] B. Meunier, Chem. Rev. 92 (1992) 1411–1456.
[8] C.J. Burrows, J.G. Muller, Chem. Rev. 98 (1998) 1109–1152.
[9] L.F. Povirk, in: S. Neidle, M. Warning (Eds.), Molecular Aspects of Anti-cancer Drug Action, Verlag-Chemie, Weinheim, Germany, 1983, p. 157.
[10] L.F. Povirk, Mutat. Res. 257 (1991) 127–143.
[11] F. Mancin, P. Scrimin, P. Tecilla, U. Tonellato, Chem. Commun. (2005) 2540–2548.
[12] P.B. Dervan, Science 232 (1986) 464–471.
[13] P.G. Schultz, P.B. Dervan, J. Biomol. Struct. Dyn. 1 (1984) 1133.
[14] J.K. Barton, J. Biomol. Struct. Dyn. 1 (1983) 621.
[15] S. Neidle, Z. Abraham, CRC Crit. Rev. Biochem. 17 (1984) 73.
[16] B.P. Hudson, J.K. Barton, J. Am. Chem. Soc. 120 (1998) 6877–6888.
[17] J.K. Barton, Science 223 (1986) 727–734.
[18] A. Spassky, D.S. Sigman, Biochemistry 24 (1985) 8050–8056.
[19] P. Hendry, A.M. Sargeson, Prog. Inorg. Chem. 38 (1990) 201.
[20] A.N. Modak, J.K. Gard, M.C. Merriman, K.A. Winkler, J.K. Bashkin, M.K. Stern, J. Am. Chem. Soc. 113 (1991) 283–291.
[21] E.L. Hegg, J.N. Burstyn, Coord. Chem. Rev. 171 (1998) 133–165.
[22] A. Sitlani, E.C. Long, A.M. Pyle, J.K. Barton, J. Am. Chem. Soc. 114 (1992) 2303–2312.
[23] D.K. Chand, H.J. Schneider, A. Bencini, A. Bianchi, C. Georgi, S. Ciattini, B. Valtancoli, Chem. Eur. J. 6 (2000) 4001–4008.
[24] C. Sissi, F. Mancin, M. Gatos, M. Palumbo, P. Tecilla, U. Tonellato, Inorg. Chem. 44 (2005) 2310–2317.
[25] A. Bencini, E. Berni, A. Bianchi, C. Giorgi, B. Valtancoli, D.K. Chand, H.J. Schneider, J. Chem. Soc., Dalton Trans. 5 (2003) 793–800.
[26] S. Mahadevan, M. Palaniandavar, Inorg. Chem. 37 (1998) 3927–3934.
[27] M. Chikira, Y. Tomizava, D. Fukita, T. Sugizaki, N. Sugawara, T. Yamazaki, A. Sasano, S. Shindo, M. Palaniandavar, W.E. Anthroline, J. Inorg. Biochem. 89 (2002) 163–173.
[28] S. Ramakrishnan, M. Palaniandavar, J. Chem. Sci. 117 (2005) 179–186.
[29] S. Mahadevan, M. Palaniandavar, Inorg. Chem. 37 (1998) 693–700.
[30] A. Raja, V. Rajendiran, P. Uma Maheswari, R. Balamurugan, C.A. Kilner, M.A. Halcrow, M. Palaniandavar, J. Inorg. Biochem. 99 (2005) 1717–1732.
[31] T. Hirohama, Y. Kuranuki, E. Ebina, T. Sugizaki, H. Arii, M. Chikira, P. Tamil Selvi, M. Palaniandavar, J. Inorg. Biochem. 99 (2005) 1205–1219.
[32] M.J. Sanchez-Moreno, D.C. Lazarte, J.M.G. Perz, R. Carballo, J.D. Ramos, A. Castineirs, J.N. Gutierrex, Polyhedron (2003) 1039–1049.
[33] P. Uma Maheswari, M. Palaniandavar, Inorg. Chim. Acta 357 (2004) 901–912.
[34] J.G. Collins, A.D. Sleeman, J.R. Aldrich, I. Greguric, T.W. Hambly, Inorg. Chem. 37 (1998) 3133–3141.
[35] J. Marmur, J. Mol. Biol. 3 (1961) 208.
[36] J. Bermadou, G. Prativel, F. Bennis, M. Girardet, B. Mcunier, Biochemistry 28 (1989) 7268–7275.
[37] K. Itoh, H. Bernstein, Can. J. Chem. 34 (1956) 170.
[38] A.W. Addison, T.N. Rao, J. Reddijk, J. van Rijn, G.C. Veschoor, J. Chem. Soc., Dalton Trans. (1984) 1349–1356.
[39] G. Murphy, P. Nagle, B. Murphy, B. Hathway, J. Chem. Soc., Dalton Trans. (1997) 2645–2652.
[40] G. Murphy, C. Murphy, B. Murphy, B. Hathway, J. Chem. Soc., Dalton Trans. (1997) 2653–2660.
[41] P. Nagle, E. O'Sullivan, B. Hathway, J. Chem. Soc., Dalton Trans. (1990) 3399–3406.
[42] M.J. Sanchez-Moreno, D.C. Lazarte, J.M. Gonzalez-Perez, R. Carballo, J.D. Martin-Ramos, A. Castineiras, J. Niclos-Gutierrez, Polyhedron 22 (2003) 1039–1049.
[43] M. Palaniandavar, T. Pandiyan, M. Lakshminarayanan, H. Manohar, J. Chem. Soc., Dalton Trans. (1995) 455–461.
[44] B. Hathaway, M. Duggan, A. Murphy, J. Mullane, C. Power, A. Walsh, B.A. Walsh, Coord. Chem. Rev. 36 (1981) 267–324.
[45] P. Tamil Selvi, M. Murali, M. Palaniandavar, M. Kockerling, G. Henkel, Inorg. Chim. Acta 340 (2002) 139–146.
[46] M. Palaniandavar, I. Somasundaram, M. Lakshminarayanan, H. Manohar, J. Chem. Soc., Dalton Trans. (1996) 1333–1340.
[47] B.K. Santra, P.A.N. Reddy, G. Neelakanta, S. Mahadevan, M. Nethaji, A.R. Chakravarty, J. Inorg. Biochem. 89 (2002) 191–196.
[48] S.A. Tysoe, R.J. Morgan, A.D. Baker, T.C. Strekas, J. Phys. Chem. 97 (1993) 1707–1717.
[49] J.M. Kelly, A.B. Tossi, D.J. McConnell, T.C. Strekas, Nucleic Acids Res. 13 (1985) 1707.
[50] I.S. Haworth, A.H. Elcock, J. Freemann, A. Rodger, W.G.J. Richards, J. Biomol. Struct. Dyn. 9 (1991) 23–43.
[51] M.T. Carter, M. Rodriguez, A.J. Bard, J. Am. Chem. Soc. 111 (1989) 8901–8911.
[52] J.K. Barton, J.M. Goldberg, C.V. Kumar, N.J. Turro, J. Am. Chem. Soc. 108 (1986) 2081–2088.
[53] S.R. Smith, G.A. Neyhart, W.A. Karlsbeck, H.H. Thorp, New J. Chem. 18 (1994) 397.
[54] C. Hiort, P. Lincoln, B. Norden, J. Am. Chem. Soc. 115 (1993) 3448–3454.
[55] H.L. Chan, H.Q. Liu, B.C. Tzeng, Y.S. You, S.M. Peng, M. Yang, C.M. Che, Inorg. Chem. 41 (2002) 3161–3171.
[56] V. Boom, A. Rich, Biochemistry 24 (1985) 237–240.
[57] P. Uma Maheswari, M. Palaniandavar, J. Inorg. Biochem. 98 (2004) 219–230.
[58] E.J. Gabbay, R.E. Scofield, C.S. Baxter, J. Am. Chem. Soc. 95 (1973) 7850–7857.
[59] B.C. Baguley, M. LeBret, Biochemistry 23 (1984) 937–943.
[60] L. Lerman, J. Mol. Biol. 3 (1961) 18–30.
[61] G.A. Neyhart, N. Grover, S.R. Smith, W. Kalsbeck, T.A. Fairley, M. Cory, H.H. Thorp, J. Am. Chem. Soc. 115 (1993) 4423–4428.
[62] M. Cusumano, A. Giannetto, J. Inorg. Biochem. 65 (1997) 137–144.
[63] J.G. Collins, T.P. Shields, J.K. Barton, J. Am. Chem. Soc. 116 (1994) 9840–9846.
[64] P. Lincoln, E. Tuite, B. Norden, J. Am. Chem. Soc. 119 (1997) 1454–1455.
[65] B. Norden, F. Tjerneld, Biopolymers 21 (1982) 1713–1734.
[66] C.A. Detmer III, F.V. Pamatong, J.R. Bocarsly, Inorg. Chem. 35 (1996) 6292–6298.
[67] C. Liu, J. Zhou, Q. Li, L. Wang, Z. Liao, H. Xu, J. Inorg. Biochem. 75 (1999) 233–240.
[68] M. Gonalez-Alvarez, G. Alzuet, J. Borras, M. Pitie, B. Meunier, J. Biol. Inorg. Chem. 8 (2003) 644–652.
[69] D.S. Sigman, M.D. Kuwabara, C.B. Chen, T.W. Bruice, Methods Enzymol. 208 (1991) 414.
[70] E.S.G. Baron, R.H. DeMeio, F. Klemperer, J. Biol. Chem. 112 (1936) 625–640.
[71] S. Ferrer, R. Bellesteros, A. Sambartolome, M. Gonazalez, G. Alzuet, J. Borras, M. Liu, J. Inorg. Biochem. 98 (2004) 1436–1446.
[72] A.M. Thomas, M. Nethaji, S. Mahadevan, A.R. Chakravarty, J. Inorg. Biochem. 94 (2003) 171–178.
[73] R. Ren, P. Yang, W. Zheng, Z. Hua, Inorg. Chem. 39 (2000) 5454–5463.
[74] M. Komiyama, N. Takeda, H. Shigekawa, Chem. Commun. (1999) 1443–1452.
[75] N.H. Williams, B. Takasaki, M. Wall, J. Chin. Acc. Chem. Res. 32 (1999) 485–493.
[76] J. Chin, Acc. Chem. Res. 24 (1991) 145–152.
[77] T. Gajda, Y. Dupre, I. Torok, J. Harmer, A. Schweigher, J. Sander, D. Kuppert, K. Hegetschweiler, Inorg. Chem. 40 (2001) 4918–4927.